Hydrogenase-based electrode for hydrogen sensing in a fermentation bioreactor

Tetyana Kyrpel, Vita Saska, Anne de Poulpiquet, Mathieu Luglia, Audrey Soric, Magali Roger, Oksana Tananaiko, Marie Thérèse Giudici-Orticoni, Elisabeth Lojou, Ievgen Mazurenko

Hydrogenase-based electrode for hydrogen sensing in a fermentation bioreactor

Tetyana Kyrpel,[a,b] Vita Saska,[a,b] Anne de Poulpiquet,[a] Mathieu Luglia,[c] Audrey Soric,[c] Magali Roger,[a] Oksana Tananaiko,[b] Marie Thérèse Giudici-Orticoni,[a] Elisabeth Lojou,[a] Ievgen Mazurenko [a *]

[a] *Aix Marseille Univ, CNRS, BIP, Bioénergétique et Ingénierie des Protéines, UMR 7281, 31, Chemin Joseph Aiguier, CS 70071 13402 Marseille CEDEX 09, France*

[b] *Analytical Chemistry Department, Taras Shevchenko National University of Kyiv, 64, Volodymyrs'ka str., Kyiv 01060, Ukraine*

[c] *Aix-Marseille Univ, Centrale Marseille, CNRS, M2P2 UMR 7340, Europôle de l'Arbois, 13545 Aix en Provence Cedex 4, France*

Abstract

The hydrogen-based economy will require not only sustainable hydrogen production but also sensitive and cheap hydrogen sensors. Commercially available H_2 sensors are limited by either use of noble metals or elevated temperatures. In nature, hydrogenase enzymes present high affinity and selectivity for hydrogen, while being able to operate in mild conditions. This study aims at evaluating the performance of an electrochemical sensor based on carbon nanomaterials with immobilised hydrogenase from the hyperthermophilic bacterium *Aquifex aeolicus* for H_2 detection. The effect of various parameters, including the surface chemistry, dispersion degree and amount of deposited carbon nanotubes, enzyme concentration, temperature and pH on the H_2 oxidation are investigated. Although the highest catalytic response is obtained at a temperature around 60 °C, a noticeable current can be obtained at room temperature with a low amount of protein less than 1 µM. An original pulse-strategy to ensure H_2 diffusion to the bioelectrode allows to reach H_2 sensitivity of 4 µA cm^{-2} per % H_2 and a linear range between 1-20 %. Sustainable hydrogen was then produced through dark fermentation performed by a synthetic bacterial consortium in an up-flow anaerobic packed-bed bioreactor. Thanks to the outstanding properties of the *A. aeolicus* hydrogenase, the biosensor was demonstrated to be quite insensitive to CO_2 and H_2S produced as the main co-products of the bioreactor. Finally, the bioelectrode was used for the *in situ* measurement of H_2 produced in the bioreactor in steady-state.

This document is the Author's version of a Submitted Work that was subsequently accepted for publication in Biosensors and Bioelectronics after peer review. To access the final edited and published work see https://doi.org/10.1016/j.bios.2023.115106

Keywords

Bioelectrode, hydrogenase, enzymatic sensor, amperometric sensor, hydrogen detection, fermentation bioreactor

Introduction

Global climate change urges scientists to look for alternative CO_2-neutral and less polluting energy sources and carriers. Hydrogen shows high expectations as a neutral energy vector and energy storage solution (Staffell et al., 2019). The transitional storage of large hydrogen amounts generated during the production peaks and used upon need is however a cornerstone of the hydrogen economy. Moreover, being a light and explosible gas (flammability range 4 – 75 %) hydrogen represents non-negligible risks when stored in large quantities. An example of this is an explosion at the hydrogen fuel station in Norway in 2019 caused by a leak ('Nel ASA: Status update #5 regarding incident at Kjørbo', 2019). Furthermore, hydrogen is a colourless and odourless substance which makes impossible its detection by human senses and these are the points of attention that require the installation of reliable sensors to detect possible leaks.

The production of hydrogen in a sustainable way is another requirement for the hydrogen economy. Among others, (photo)electrochemical water splitting (Tee et al., 2017) but also biological methods are envisioned (Akhlaghi and Najafpour-Darzi, 2020; Hidalgo and Martín-Marroquín, 2022). In particular, hydrogen production in the dark fermentation process by a bacterium or a consortium of several bacteria from a wide range of food and agricultural feedstocks could become one of the eco-friendliest processes (Sarangi and Nanda, 2020; Xu et al., 2022). This process is developed in an anaerobic reactor due to the oxygen-sensitivity of most fermentative bacteria and H_2 production is associated to the acetate or butyrate pathways, while CO_2 is released as a co-product. Despite multiple fundamental challenges still present (Brar et al., 2022; Ghimire et al., 2015; RenNanqi et al., 2011), numerous types of bioreactors producing hydrogen have been built (Barca et al., 2015). Yet, the level of H_2-production in such bioreactors remains unstable and depends, among other factors, on the substrate used, pH and bacteria fitness. Hence, a hydrogen detector installed at the gas outlet of reactors and providing the information about the current production rate in real time seems to be an indispensable device.

The presence of hydrogen detection systems thus appears essential in the critical nodes of the future hydrogen infrastructure, at the production, use and storage points. Such systems relate

more to the sensor technology having low cost, small size and fast response than to the classical large and high-tech instruments such as gas chromatography and mass-spectrometry. Further requirements include suitable detection range, safe performance, robustness and low cross-sensitivity. It should be noted that despite an active development, no hydrogen sensors were demonstrated satisfying all the requirements postulated by the US Department of Energy (DoE) (Darmadi et al., 2020; *Multi-Year Research, Development, and Demonstration Plan 2011−2020. Section 3.7 Hydrogen Safety, Codes and Standards*, 2015). Main sensing principles have been extensively reviewed and corresponding devices commercialized (Hübert et al., 2011). They can be classified into catalytic, thermo-conductive, electrochemical, resistive, work function, mechanical, optical and acoustic types. Whatever the transducer principle, the sensing element often includes a material that changes its properties upon contact with hydrogen. Traditionally, palladium, platinum and other noble metals are used since they are efficient catalysts, have high affinity and can absorb large quantities of hydrogen. Many sensor types, *e.g.* catalytic and resistive, additionally require elevated temperatures (>100 °C) to function, which not only leads to high power consumption, but also poses security risks. Catalytic sensors also require oxygen to be present in the atmosphere and thus are not suitable for the hydrogen determination in anaerobic conditions. On the other hand, the humidity seems to affect adversely the response of the sensors too, although only few studies have investigated its impact (Darmadi et al., 2020).

As it is for the hydrogen production, an alternative to the expensive rare metals catalysts for the hydrogen detection may be found in nature. The ability to catalyse hydrogen oxidation is an intrinsic property of hydrogenases, one of the most studied redox enzymes (Lubitz et al., 2014). There were few attempts to explore this ability of hydrogenases to detect hydrogen. In one of the first works, Qian *et al* developed an electrochemical mediated sensor by entrapping hydrogenase from *T. roseopersicina* and poly(butylviologen) mediator between two clay layers. A sensitivity in the order of 1 μA cm^{-2} per % H_2 was achieved, but a slow response time of tens of minutes was also noted (Qian et al., 2002). Lutz *et al* used an O_2-tolerant hydrogenase from *R. eutropha* to develop a mediated chronoamperometric biosensor capable to detect H_2 in the 1-100% range with currents in the range of 1-2 μA cm^{-2} per % H_2 (Lutz et al., 2005). The method involved however toxic benzyl viologen as a dissolved mediator. Alonso-Lomillo *et al* manufactured multiwalled carbon nanotubes (MWCNT) modified gold electrodes, and employed them as a platform for the immobilisation of the O_2-sensitive hydrogenase from *D. gigas* allowing high currents for hydrogen oxidation with sensitivity of 2 μA cm^{-2} per μM H_2

when the electrode was rotating at 2500 rpm (Alonso-Lomillo et al., 2007). Besides an artificial convection required to achieve such activity, the O_2-sensitivity of the hydrogenase from *D. gigas* limits considerably the application scope of such a sensor. This is also most probably one of the reasons why so few reports on the enzymatic hydrogen sensors can be found in the literature, the majority of hydrogenases requiring strict anaerobic conditions for manipulations.

Membrane-bound hydrogenase I from the hyperthermophilic bacterium *Aquifex aeolicus* (*Aa* Hase) has been shown previously to possess promising features for biotechnological applications, such as thermostability, H_2 affinity, O_2- and CO-tolerance (Brugna-Guiral et al., 2003; Luo et al., 2009). Several generations of H_2/O_2 fuel cells have been notably reported featuring *Aa* Hase anode (Ciaccafava et al., 2012b; Mazurenko et al., 2017; de Poulpiquet et al., 2014). The outstanding properties of *Aa* Hase combined with the already acquired knowledge of its functioning at electrochemical interfaces suggest the enzyme could be advantageously used as a sensing element.

In this work we developed an immobilisation platform and explored the prospects of *Aa* Hase as a key element of an amperometric hydrogen biosensor, suitable in particular for the H_2 quantification at the biogas outlet of an anaerobic bioreactor. We optimised the bioelectrode fabrication based on a simple procedure of CNT-modification and enzyme adsorption. This bioelectrode was further tested at different conditions, and calibration curves were obtained in the forced-convection and stationary conditions. The impact on the detection of main interferents known to be produced in the reactor was studied. Finally, the developed biosensor was employed for the quantification of the biohydrogen produced in a dark fermentation bioreactor while the results were compared with gas chromatography.

Experimental part

Materials and reagents

Potassium hydrogen phosphate (99%), potassium dihydrogen phosphate (99%), potassium hydroxide (KOH), sodium sulphide (Na_2S) were purchased from Fisher Scientific, N-methyl-2-pyrrolidone (NMP, 99.5%) was from Acros Organics.

Non-functionalized (MWCNT) CNTs were from Nanocyl, Belgium (Nanocyl 3100). NH_2-functionalized CNTs (MWCNT-NH_2) were from Dropsens, Spain (DRP-MWCNTNH2). COOH-modified CNTs were purchased from NanoLab, USA (PD15L1-5 COOH).

N_2 and CO_2 high purity gases were supplied from Linde, France. Hydrogen with declared purity > 99.99995% was produced in a generator Parker Domnick Hunter 110H-MD, UK.

Membrane-bound [NiFe]-hydrogenase from *Aquifex aeolicus* (*Aa* Hase) was purified according to the procedure described previously (Brugna-Guiral et al., 2003).

Electrode preparation

Carbon nanotubes were dispersed in NMP (MWCNT and MWCNT-NH_2) or MilliQ water (MWCNT-COOH) at the concentration 1 mg mL^{-1} by ultrasonication for 4 h (NMP) or 1 h (water). Pyrolytic graphite (PG) electrode (Ø 3 mm) was masked with a Parafilm o-ring mask leaving only the electrode surface available for the dispersion. 5 µL of the CNT-dispersion was dropped on the electrode surface and dried under the vacuum for at least 5 min until the solvent was completely evaporated. In the case of water-based dispersion, the electrode was dried for 15 min at 60 °C. The last step was repeated several times if necessary. Then, 5 µL of *Aa* Hase solution was deposited on the electrode surface, covered with a microtube to avoid evaporation and placed in the fridge at 4 °C for the adsorption. Before electrochemical study the electrode was rinsed with MilliQ water and immediately placed in the electrochemical cell.

Electrochemical experiments

Electrochemical measurements (Cyclic voltammetry (CV), and chronoamperometry) were performed in a standard 3-electrode cell (comprising a modified PG as a working electrode, a Hg/Hg_2SO_4 reference electrode (sat. K_2SO_4) and a Pt-wire auxiliary electrode) using a potentiostat from Metrohm-Autolab PGSTAT101 controlled by Nova 2.1 software (Eco Chemie). All potentials are quoted vs normal hydrogen reference electrode (NHE) by adding 620 mV to the measured potential. Scan rate was 10 mV s^{-1} for all CV experiments. Current densities are reported to the geometrical surface of the electrode (0.071 cm^2). All experiments with electrode rotation were performed on the Metrohm-Autolab rotating ring-disk system with a home-made glassy carbon electrode (GC) tip with similar surface area.

Phosphate buffer with pH 7.0 and concentration 0.1 M and temperature 25±1 °C was used as an electrolyte, unless mentioned otherwise. The solution in the electrochemical cell was

continuously bubbled with pure gases or mixtures with various ratios. The necessary gas ratios were created using two flow meter controllers (Sierra Instruments) with different scales allowing to cover the range 0.04 – 50 %.

Scanning electron microscopy

The electrode samples were observed by a Vega3 Tescan scanning electron microscope (SEM). An accelerating voltage of 10 keV with a working distance of 5 mm was used.

Dynamic light scattering

Dynamic light scattering (DLS) to determine the size of dispersed particles was performed using Malvern ZetaSizer Nano ZS, UK. Due to the high optical absorbance of CNT-dispersions, a 10-times dilution was performed before the measurement. Back scattering detection at an angle 173° was used and three replicate measurements were systematically made.

Bioreactor setup

An up-flow anaerobic packed-bed bioreactor of 5 L (Minifors 1, Infors), working volume of 3 L, was set up for the experiments. The bioreactor was packed with Kaldnes K1 as biofilm carriers and the porosity of the packed-bed was 84%.

The bioreactor was operated according to a continuous up-flow of about 0.78 L h^{-1} of medium, thus leading to a hydraulic retention time of about 3.4 h. An internal recirculation of the culture from the top to the bottom of the bioreactor was applied at a flow of 15 L h^{-1}. The bioreactor was stirred at the bottom with Rushton impeller at 300 rpm. N_2 gas was continuously sparged at the bottom of the bioreactor at a flow of 3 L h^{-1}. The temperature was controlled at 37 °C and the pH was regulated at 5.8 by addition of 1.5 N NaOH in the headspace.

The medium used for the experiments consisted of (for 1 L): K_2HPO_4 (0.5 g), NH_4Cl (2 g), yeast extract (1 g), D-glucose (2.5 g), and trace element stock solution 1000X (1 mL). The bioreactor was inoculated with a synthetic consortium of two strains: *Clostridium acetobutylicum* ATCC824 and *Desulfovibrio vulgaris* Hildenborough DSM644 at 1:1 ratio (O.D.).

After inoculation step, the bioreactor was operated in batch mode during 22 h. Then a D-glucose stock solution was added to a final concentration of 2.5 g L^{-1} in the bioreactor, thus operating in fed-batch mode during 20 h. After this period the bioreactor was turned in continuous mode.

At the gas outlet of the bioreactor, the gas flow rate was recorded every 5 min using a volumetric gas meter (drum-type gas meter TG0.5, Ritter). Then downstream the gas composition was measured each hour by gas chromatography (MicroGC 490, Agilent), previously calibrated and operating in continuous flow. The MicroGC was equipped with thermal conductivity detector with two modules consisted of: a module A with a backflush injector heated at 95 °C, a 5 m PBQ + 10 m MS5A column heated at 145 °C with Ar as the gas carrier, and a module B with a variable injector heated at 95 °C, a 10 m PPU column heated at 70 °C with He as the carrier gas.

Results and Discussions

Electrocatalytic response as a function of CNT type. The electrode surface plays an important role in enzyme electrochemistry. Since the rate of interfacial electron transfer decays in an exponential manner with the increase of the distance to the electrode, only a monolayer of adsorbed redox proteins can be practically electroactive. On the other hand, enzyme molecules are rarely of spherical shape with an active centre in the middle, so that the configuration in which the enzyme molecule is adsorbed on the electrode surface plays a role by modifying the electron tunnelling distance. The surface of the electrode has to be tuned to favour the adsorption in the configuration with the shortest distance between enzyme and the active centre. In line with our previous findings of the importance of electrostatic interactions (Mazurenko et al., 2016; Monsalve et al., 2016), we have tested different types of MWCNTs as a support for *Aa* Hase immobilisation. Pristine non-modified MWCNTs, COOH-modified and NH_2-modified MWCNTs were notably tested. The properties of all MWCNTs, notably the zeta-potential, elemental composition and size, were reported earlier (Hitaishi et al., 2020; Mazurenko et al., 2016). While pristine MWCNTs and COOH-modified MWCNTs were already evaluated as surface modifiers for *Aa* Hase immobilisation (Monsalve et al., 2016), MWCNTs covalently-modified with NH_2-groups have not been yet used with this enzyme. To

facilitate the comparison, the same quantity of all MWCNT types was deposited on the PG-electrode.

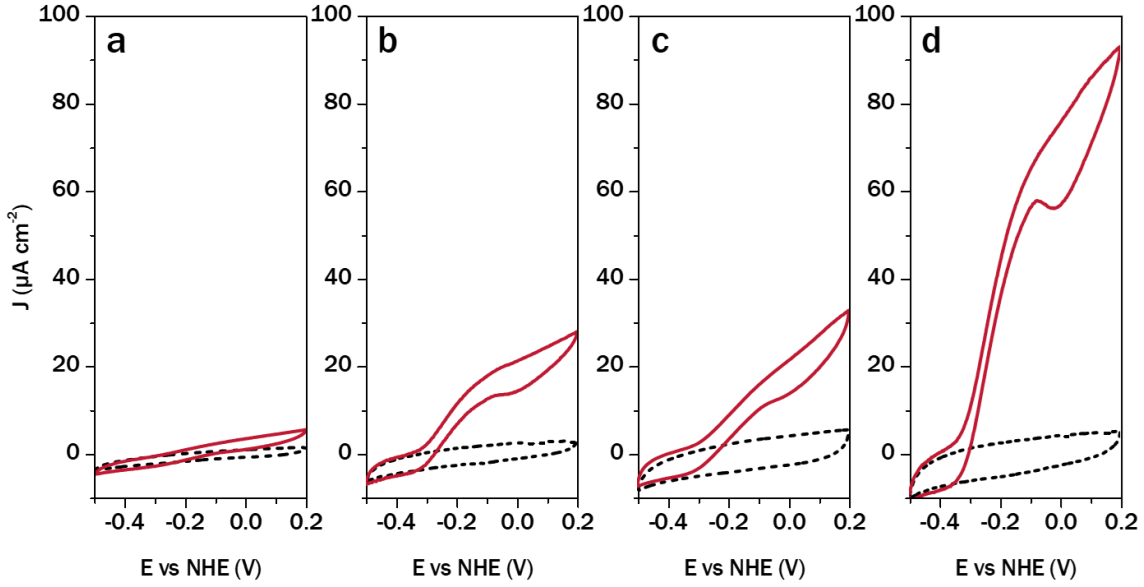

Figure 1. Cyclic voltammograms of different electrodes modified with *Aa* Hase under (black dashed line) N_2 and (red line) H_2 atmosphere: a) PG, b) PG-MWCNT, c) PG-MWCNT-COOH, d) PG-MWCNT-NH_2. Amount of *Aa* Hase used for modification: 5 µL of 20 µM. Supporting electrolyte: Phosphate buffer pH 7 (0.1M), 40 °C

As it is evidenced from Figure 1, when modified with *Aa* Hase all electrode types demonstrate a well-defined anodic catalytic current in the presence of H_2 with apparent onset potential -0.3 - -0.35 V *vs* NHE. This catalytic current is related to the H_2 oxidation by [NiFe] active centre of *Aa* Hase which proceeds through H_2 binding to Ni-SI_a state and heterolytic cleavage with formation of a bridging hydride (Ni-R state). The consecutive transfer of two electrons to the proximal [FeS]-cluster and a proton release results first in a Ni-C state and then in the restoration of the initial Ni-SI_a state (Lubitz et al., 2014). At higher potentials, a slope change and a momentary current increase on the backward scan at -0.05 V are observed. This corresponds to the reversible deactivation-reactivation process of *Aa* Hase as a function of the potential. The process is known for all characterised [NiFe]-hydrogenases and it is explained by the formation of the inactive Ni-B state of the active centre when scanning toward higher potentials and its reduction when scanning back (Vincent et al., 2007). The MWCNTs enhance the electrode surface area, as attested by the capacitive current increase under N_2. This allows more enzymes to be adsorbed and to participate in the catalysis, giving rise to the catalytic current enhancement at least 5-times compared with the non-modified electrode (Figure 1, red lines). It should be noted however that despite a similar capacitive current, *i.e.* similar amount of MWCNT deposited, catalytic current enhancement varies with MWCNT type, spanning

from 25-30 µA cm^{-2} in the cases of MWCNT and MWCNT-COOH to 90 µA cm^{-2} in the best case of MWCNT-NH_2. Such difference between positively- and negatively-charged CNTs has been already observed earlier for *Aa* Hase, except that positively-modified CNTs were prepared by non-covalent modification by Pyrene-NH_2 molecules (Monsalve et al., 2016). Interestingly, the current is enhanced by the same factor of *ca.* 3 irrespective of the way the positive charge is introduced on the CNT-walls. This can be explained by the weak fluctuating dipole moment of *Aa* Hase that displays large direction variations but still points predominantly away from the distal [FeS]-cluster (Oteri et al., 2014). This property allows *Aa* Hase to display a higher catalytic current on positively-charged CNTs while also being somewhat active on negatively-charged CNTs. In consequence, MWCNT-NH_2 were used for all further studies. The process of electrode modification was also characterised step-by-step by cyclic voltammetry and electrochemical impedance spectroscopy (Figure S1, Figure S2) using $K_3[Fe(CN)_6]$ / $K_4[Fe(CN)_6]$ couple as a redox probe. When PG is modified with MWCNT-NH_2, an increase of the apparent electron transfer constant is observed, which doesn't change significantly upon *Aa* Hase immobilisation (Table S1) suggesting that the large enzyme molecules cannot block completely the CNT-surface from small diffusing probes.

Optimization of *Aa* Hase adsorption. In order to maximise the catalytic current while keeping the amount of the adsorbed enzyme as low as possible, the optimal concentration of the deposited enzyme solution was investigated. The dependence of the catalytic current on the enzyme concentration should have a form of Langmuir isotherm with a saturation in the region where an electroactive monolayer of adsorbed enzymes is completed. In our case, this dependence had a peak-shaped form with both low and high concentrations yielding to the drop of the catalytic current (Figure 2A). The optimum was obtained with 0.5 µM *Aa* Hase, highlighting that a very low amount of protein is required for H_2 detection. While unusual, such dependence was already observed *e.g.* for *M. verrucaria* bilirubin oxidase on planar gold electrodes where it was explained by the formation of more crowded and sterically-hindered adlayer at higher concentrations (McArdle et al., 2015). While the same reasoning can be applied here, in the particular case of *Aa* Hase such dependence can have two additional possible explanations: a) after purification, *Aa* Hase sample contains a non-negligible amount of surfactant (DDM) which helps the membrane-bound enzyme to maintain its structure and functions (Ciaccafava et al., 2012a). The surfactant itself should interact with the partially hydrophobic MWCNTs. With sample dilution the concentration of the surfactant drops and this may lead to the micelle restructuration and, in turn, to the change of the adsorption mechanism;

b) since *Aa* Hase was purified without affinity tags, the purity of the final sample remains lower than 90% (Figure S3). Some low-concentration impurities might have higher affinity for the MWCNT-NH_2 surface than *Aa* Hase. Even if their amount is not sufficient to block the electrodes surface when the diluted samples are used, they may hinder the adsorption of the enzyme from the concentrated solutions, possibly leading to the catalytic current drop as observed on the Figure 2A. The fact that a catalytic current can be observed even from the enriched protein samples should be considered as an advantage for biotechnologies since high purity proteins can hardly be obtained after a native enzyme purification. It must be however emphasized that the induced catalytic current may vary as a function of the enzyme fraction.

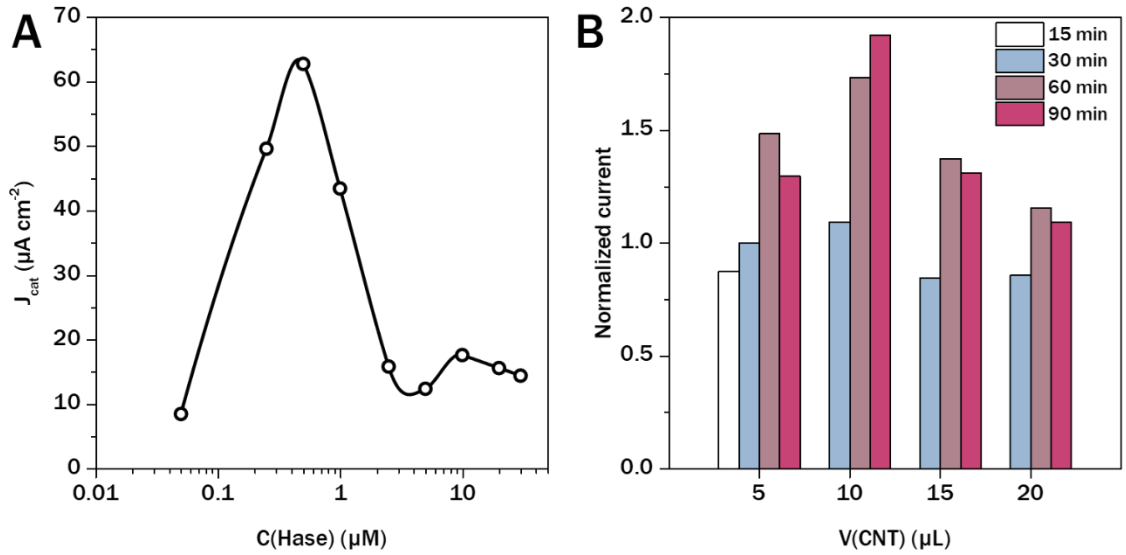

Figure 2. (A) Magnitude of the catalytic current of H_2 oxidation by *Aa* Hase modified PG-MWCNT-NH_2 electrode at -0.1 V *vs* NHE and as a function of enzyme solution concentration. Phosphate buffer pH 7 (0.1M), 25 °C, V_{MWCNT} = 5 µL, V_{enzyme} = 5 µL, adsorption for 30 mins at 4 °C. (B) Normalized catalytic current at -0.1 V *vs* NHE of H_2 oxidation by *Aa* Hase modified PG-MWCNT-NH_2 electrode as a function of MWCNT quantity and adsorption time. Phosphate buffer pH 7 (0.1M), 25 °C, V_{enzyme} = 5 µL, C_{enzyme} = 0.5 µM.

The optimal concentration 0.5 µM of the *Aa* Hase was used for all further experiments. On the next step, the amount of CNTs and the enzyme adsorption time was optimised. It is safe to suggest that more CNTs should increase the amount of the adsorbed and electroactive enzyme molecules while longer adsorption time should ensure that the enzyme molecules have diffused inside the porous layer and an adsorption equilibrium has been reached. Although this tendency is confirmed (Figure 1B), the maximal current gain of 200 % only could be obtained upon the optimization. One hour was sufficient to reach equilibrium and longer adsorption time didn't lead to the signal enhancement, except for the slight increase at 10 µL of CNT. Interestingly, the maximal response was obtained when 10 µL of CNT suspension was used while larger

quantities didn't enhance the response and even led to its decrease. The explanation might be found in the increased thickness of the porous layer that prevents hydrogen from the solution to reach the enzymes immobilised deep inside. This is coherent with the observation that the current stays almost the same for 30 min of adsorption irrespective of the total layer thickness since the enzyme molecules have time to penetrate only to a certain depth during this time. It should be noted that although 60 min of adsorption showed higher current, some further experiments were performed with 30 min of adsorption to mitigate a higher dependence on the CNT quantity observed at 60 min.

Temperature influence. *Aa* Hase being extracted from a hyperthermophilic organism is known to demonstrate an activity enhancement at elevated temperatures that may go up to 85-90 °C (Brugna-Guiral et al., 2003; Lojou et al., 2005; Monsalve et al., 2016). To evaluate the performance of the sensor at higher temperatures, we performed a CV on the same electrode in the temperature range from 30 to 60 °C (Figure S4). A 4-fold activity enhancement was observed when the temperature was changed from 30 to 60 °C, in agreement with previous reports (Monsalve et al., 2016).

Influence of CNT-dispersion. Due to their aspect ratio and high hydrophobicity, pristine CNTs are hardly dispersible in the aqueous media. The use of organic solvents and ultrasonication are necessary to separate the individual tubes and even then, the dispersions can deteriorate with time. Decrease of the magnitude of the bioelectrode response was observed when the dispersion was used repeatedly for the electrode modification for 1 month (Figure 3A). On average, the response was decreased by 33 % when a 1-month old dispersion was used compared to a fresh one. Since visually the dispersion did not change its appearance during this time, dynamic light scattering (DLS) experiments were performed to estimate the dispersion degree in both cases. The DLS measurements show the disappearance of the individually

dispersed CNTs (peak at 20-30 nm) and formation of larger aggregates (peak at 400-600 nm) due to a partial aggregation (Figure 3B).

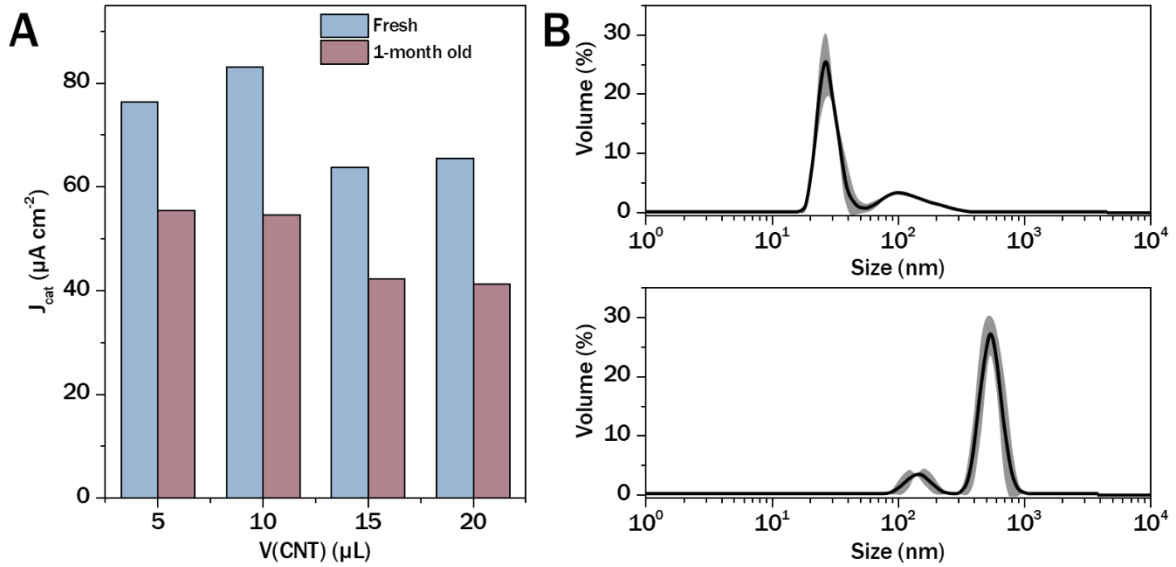

Figure 3. Influence of the CNT dispersion quality. (A) Catalytic current density of *Aa* Hase modified PG-MWCNT-NH_2 at -0.1 V *vs* NHE as a function of CNT dispersion volume and quality. Phosphate buffer pH 7 (0.1M), V_{enzyme} = 5 µL, C_{enzyme} = 0.5 µM, adsorption for 30 mins at 4 °C. (B) Distribution of the particles sizes measured by DLS in (top) freshly prepared and (bottom) 1-month old CNT dispersion.

The difference between fresh and partially aggregated CNT-dispersions is visible also on the SEM-images of the deposit (Figure S5). Indeed, more aggregates can be distinguished on the low-magnification images. It can be speculated that partial aggregation impedes the formation of pores suitable for enzyme size upon deposition. It was noticed however that such aggregation occurs only when the dispersion was repeatedly used, *i.e.* the recipient was opened and closed. These changes were not observed with the MWCNT-NH_2 dispersion that was tightly sealed for at least several months.

Reproducibility of the bioelectrode fabrication. The reproducibility of the bioelectrode fabrication was estimated by comparing two following characteristics: a) the electroactive surface area of the CNT-deposit was calculated from the capacitive current measured at various scan rates in the absence of H_2 (Figure S6) and b) the electrocatalytic current generated by bioelectrode measured in the same conditions (Figure 4). The procedure of the electrode modification by CNTs has satisfactory reproducibility with relative standard deviation of electroactive area not exceeding 10 % for 9 individual electrodes. The average electroactive surface area of PG-MWCNT-NH_2 modified with 10 µL of CNT-dispersion was 5.89 cm^2 and the roughness factor was 83 compared with the geometrical area of bare PG-electrode.

Regarding the reproducibility of the modification by *Aa* Hase, the average bioelectrode current density was 75.6 µA cm^{-2} with standard deviation 8 % for 6 electrodes.

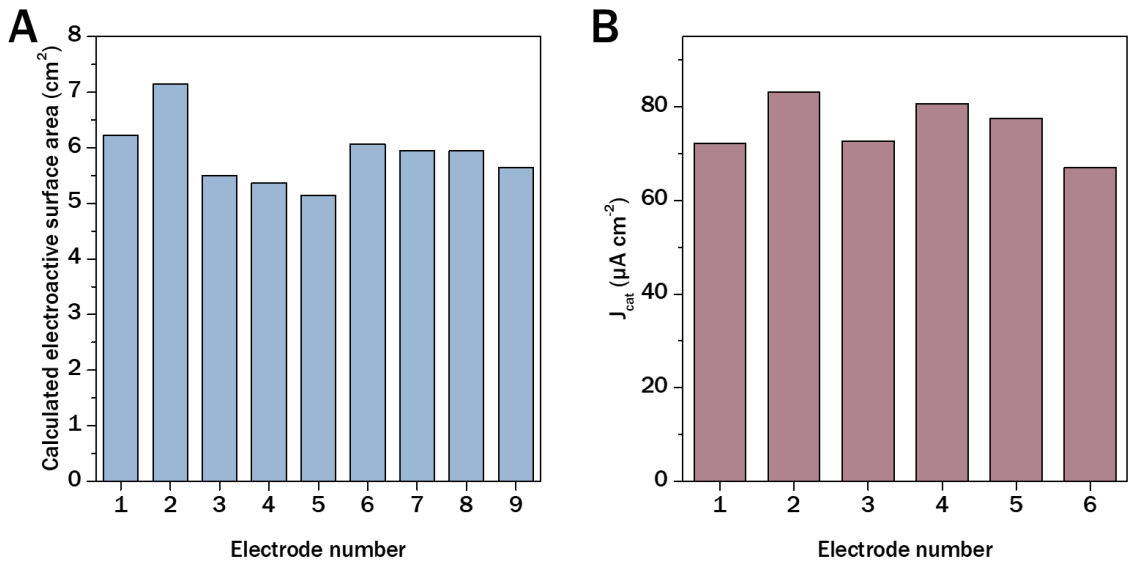

Figure 4. Reproducibility of the bioelectrode fabrication. (A) Reproducibility of the CNT-deposit electroactive surface area upon deposition of 10 µL of dispersion at different electrodes. (B) Reproducibility of the electrocatalytic response (at -0.1 V *vs* NHE) at different electrodes at 100 % H_2. V_{MWCNT} = 10 µL, V_{enzyme} = 5 µL, C_{enzyme} = 0.5 µM, adsorption for 30 mins at 4 °C.

Michaelis constant. The sensitivity and the detection limit of a biosensor depend on the intrinsic properties of the enzymatic component, notably activity and Michaelis constant. As a general rule, higher activity and lower Michaelis constant should lead to a better catalytic efficiency and thus higher biosensor sensitivity. At the same time, the response can be considered linear in the substrate concentration range between 0 and K_M. It should be noted however that in practice multiple other factors play a role. K_M of 3 µM H_2 for *Aa* Hase at 25 °C was reported before based on unpublished data. We refined this value by performing triplicate chronoamperometric measurements using a method described before (Léger et al., 2004). The measured apparent K_M of the immobilised *Aa* Hase to H_2 at -0.15 V (*vs* NHE) was found to be 9.8 ± 0.6 µM (Figure S7), which corresponds to 1.3 % H_2. This means that *Aa* Hase theoretically is suitable for the determinations of H_2 quantities much below the lower explosion limits (4 %) with a limit of detection discussed hereafter.

Calibration. Besides Michaelis constant, mass transfer is another important factor which determines the sensitivity and the linear range of the enzymatic biosensor. Since equilibrium hydrogen concentration in an aqueous solution in contact with a gas mixture at the lower explosivity limit (4% H_2) is only 31.2 µM at 25° C, the enzymatic activity will result in its fast

depletion near the electrode surface and thus signal drop. Hence, the mass transfer should be enhanced in order to improve the sensitivity of the sensor to low concentrations. To facilitate this process, we first explored the performances of two different usual approaches, gas bubbling into the solution with a stationary electrode and electrode rotation.

The CVs obtained on the stationary electrode under gas bubbling in the cell were rather noisy and characterised by low reproducibility (Figure S8), especially in the range 2.5-10 % H_2. This can be explained by the inhomogeneous solution stirring by the gas bubbles, and as a result concentration fluctuation near the electrode. Despite the noise, a linear dependence of the current at -0.1 V (*vs* NHE) on H_2 content was observed in the range 1 - 10% H_2 with a sensitivity of 6.6 ± 0.6 µA cm^{-2} per % H_2 (Figure 5B).

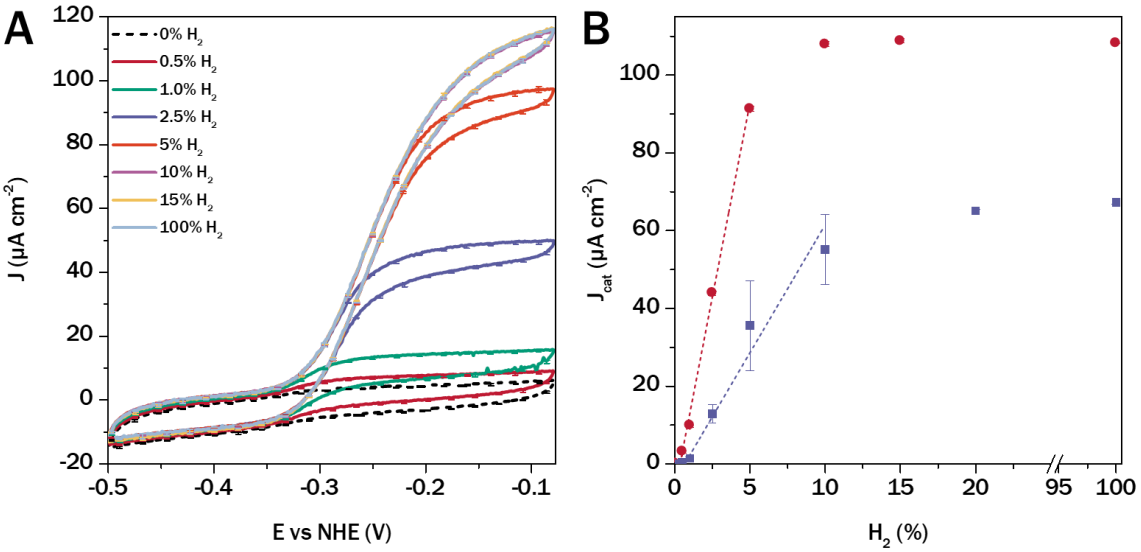

Figure 5. Calibration curves. (A) Averaged CVs of the *Aa* Hase modified RDE GC-MWCNT-NH_2 under various hydrogen content on RDE (2000 rpm); Phosphate buffer pH 7 (0.1M), V_{MWCNT} = 10 µL, V_{enzyme} = 5 µL, C_{enzyme} = 0.5 µM, adsorption for 30 mins at 4 °C; (B) Dependence of the catalytic current at -0.1 V (NHE) on the H_2 concentration without (blue squares) and with electrode rotation (red circles). Dashed lines indicate approximative linearity zone. Error bars represent standard deviations for four identical cycles.

When a rotating disk electrode (RDE) was used, the CVs demonstrated much lower noise level (Figure 5A) and higher sensitivity. The response was linear in the 0.5 -5 % H_2 range with sensitivity 20.0 ± 0.9 µA cm^{-2} per % H_2. This can be explained by enhanced mass transfer and well-defined diffusion profile characteristics of RDE. It should be also noted that half of the maximal response on RDE is observed at H_2 concentrations (*ca*. 2.5 %) which are much closer to previously determined K_M (1.3 %).

Pulsed detection at stationary electrode. Despite enhanced sensitivity and lower detection limit obtained on the RDE, it is difficult to imagine the employment of such cumbersome and energy-consuming systems in real sensors. A flow-method should give a similar diffusion enhancement but requires an additional energy input as well. We therefore tried to change the detection method to avoid any mechanical forced convection while maintaining the sensor characteristics. For this, we had recourse to pulsed detection with applied potential changing periodically from the value where the reaction takes place to the one where there is no reaction that allows to restore the diffusion layer. Two potentials were chosen: -0.1 V at which the activity is reasonably high but strong potential deactivation is not observed yet, and -0.4 V at which the H_2 oxidation doesn't take place thus allowing the diffusion layer to be restored. Furthermore, the lower potential allows it to reactivate any potentially inactivated fraction of *Aa* Hase. Then, the duration of the pulse was optimised by performing long 30 s-pulses and sampling the current at different time points from the pulse start (Figure 6).

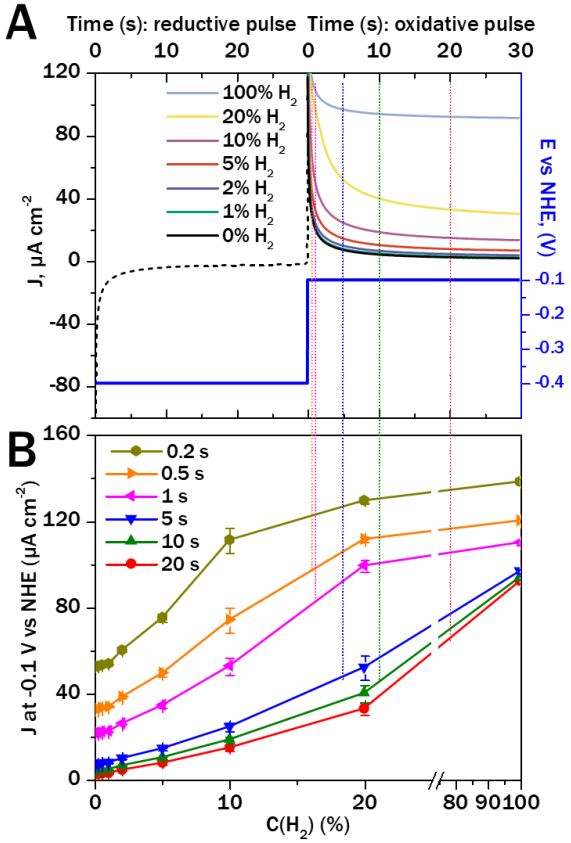

Figure 6. Pulsed detection. (A) One chronoamperometric pulse sequence of the *Aa* Hase modified PG-MWCNT-NH_2 under various hydrogen content: the potential applied during the sequence is shown as blue curve; the current recorded during the reductive pulse, which is identical for any hydrogen content, is shown as a black dashed curve; the current recorded during the oxidative pulse is shown as solid coloured curves, depending on the hydrogen content; (B) Dependence of the current density sampled at different time points from the oxidative

pulse start on the hydrogen content in the cell. Error bars represent standard deviations for nine identical pulses. Phosphate buffer pH 7 (0.1M), V_{MWCNT} = 10 µL, V_{enzyme} = 5 µL, C_{enzyme} = 0.5 µM, adsorption for 60 min at 4 °C.

The recorded current reveals the contribution of two processes: the charging current which depends on the active surface area and exponentially decays with time; and the faradaic current which depends on the concentration of the dissolved hydrogen and decays with square root of time. This dependence has a complex nature dictated by the enzymatic activity and hydrogen diffusion. Two cases can be identified depending on the current sampling moment. At shorter sampling time less than 0.5 s, the bioelectrode has higher sensitivity to the hydrogen *ca.* 4 µA cm^{-2} per % H_2 but smaller linearity range 1-10 % (Figure 6, Figure S9). The levelling of the current response above 10 % can be explained by concentrations of the hydrogen significantly exceeding the Michaelis constant of the hydrogenase. At longer sampling times more than 1 s the sensitivity of the bioelectrode gradually decreases and levels at *ca.* 1.3 µA cm^{-2} $\%^{-1}$ while the linearity range extends towards higher concentrations (Figure S9). The longer the oxidative potential is applied to the bioelectrode the more hydrogen gets depleted in the vicinity of the electrode and the more important contribution of the diffusion becomes. Thus, the duration of the pulses can be adjusted depending on the expected hydrogen content: the shorter pulses can be used to detect traces of H_2 with high sensitivity, while longer pulses allow to extend the linear range and quantify higher H_2-content.

Interferences study. Various gaseous substances can be found together with hydrogen in real samples. Some of them can cause cross-selectivity and/or poisoning of the noble metal-based sensors, *e.g.* CO, SO_2 and H_2S. *Aa* Hase is known to be resistant to CO due to its weak binding with [NiFe]-centre (Luo et al., 2009; Pandelia et al., 2010). In the dark fermentation process, traces of H_2S are more likely to be produced than SO_2, and CO_2 is additionally co-produced together with H_2. The mechanism of H_2S inhibition of [FeFe]-hydrogenases was recently elucidated (Felbek et al., 2021; Rodríguez-Maciá et al., 2018). Sulphide-inhibition at oxidative potentials was also demonstrated for several [NiFe]-hydrogenases (Vincent et al., 2006). We therefore investigated the influence of sulphide on the catalytic signal of the biosensor by introducing Na_2S into the electrochemical cell. Since the second pKa of H_2S lies between 12 and 17 and the first pKa is equal to 7, Na_2S is completely hydrolysed in the aqueous solutions with formation of H_2S and HS^- (Li and Lancaster, 2013). We have chosen a more acidic pH 6 for the interference experiments because at this pH 90 % of the added sulphide is found in the

form of solubilized H_2S (aq) immediately after the injection. The current of the modified bioelectrode itself remains stable between pH 6 and 7 (Figure S10).

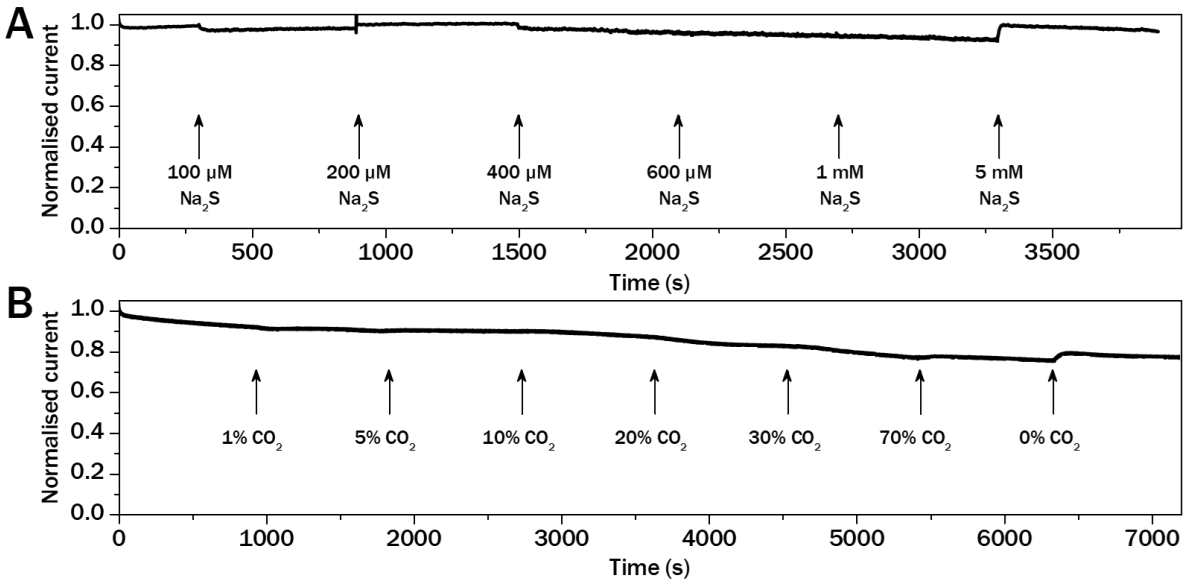

Figure 7. Chronoamperograms of the *Aa* Hase modified PG-MWCNT-NH_2 under H_2 atmosphere upon (A) Na_2S additions and (B) mixing with CO_2. Applied potential (A) 0.0 V *vs* NHE or (B) -0.1 V *vs* NHE, 0.1M phosphate buffer pH 6. V_{MWCNT} = 10 µL, V_{enzyme} = 5 µL, C_{enzyme} = 0.5 µM, adsorption for 30 mins at 4 °C.

The chronoamperogram of the *Aa* Hase modified electrode doesn't demonstrate clear response to the sulphide additions for concentrations up to 5 mM (Figure 7A). At 5 mM of Na_2S a 10 % current increase was observed which can be probably attributed to the beginning of a sulphide oxidation process. We conclude therefore that sulphides and H_2S do not interfere with hydrogen detection by the developed bioelectrode at sub-millimolar concentrations and that *Aa* Hase itself is less sensitive to sulphides than other [NiFe]-hydrogenases.

The amount of CO_2 produced during dark fermentation can be the same or even exceed the quantity of H_2 (Barca et al., 2015). Even though CO_2 is not supposed to be reduced directly on the electrode unless poised at very negative potentials, it might represent an interfering action by lowering the solution pH and thus influencing enzyme activity due to the solubilization and reaction with water: $CO_2 + H_2O \Leftrightarrow H^+ + HCO_3^-$. A sufficient buffer concentration is required to compensate for this possible pH decrease. We simulated the conditions of the bioreactor outlet by mixing-in higher and higher CO_2-amounts to the H_2. Chronoamperometric response is given in Figure 7B, the current was nearly stable before 20% CO_2. Current increase around 5 % after each step was observed from 20 % CO_2 that was partially restored after the return to 100 % H_2. It should be noted that the concentration of H_2 in this experiment was decreasing

with an increase of CO_2 percentage. Thus, the observed current drop should rather originate from the decrease of the substrate concentration than CO_2-inhibition. pH decrease might be another reason but the pH in the cell was lowered from 6 to only 5.86 after almost 2 hours of the experiment and such little pH change is unlikely to influence significantly the response.

Detection of the hydrogen in a lab-scale dark fermentation bioreactor. To test the feasibility of the hydrogen detection by the developed biosensor we connected the electrochemical cell at the gas outlet of the 3 L packed-bed bioreactor. This bioreactor employs the syntrophic association of two bacteria which are naturally involved in the process of biological hydrogen production from organic matter in anoxic environments: *Clostridium acetobutylicum* and *Desulfovibrio vulgaris*. The former carries out dark fermentation using glucose as substrate while producing volatile fatty acids and hydrogen (maximum yield of 4 H_2 produced per mole of glucose utilised) and carbon dioxide. While *C. acetobutylicum* is thought to be the main hydrogen producer in this system, previous studies demonstrated that hydrogen production is improved in the presence of *D. vulgaris* (Benomar et al., 2015). Whether *D. vulgaris* directly participates in hydrogen production (through the activity of its periplasmic and membrane-bound hydrogenases) or indirectly contributes to improve hydrogen yields by rewiring *C. acetobutylicum* metabolism remains unclear. Nevertheless, it was shown that anaerobic packed-bed bioreactor inoculated with a co-culture of *C. acetobutylicum* and *D. vulgaris* continuously fed with glucose give a continuous and stable hydrogen production (Barca et al., 2016).

The electrochemical cell was connected to the gas outlet in parallel after a 3-way valve allowing to direct the gas flow either through the cell or to the gas chromatograph omitting the cell (Figure 8A, Figure S11). Such configuration allowed to perform biosensor and cell manipulations without disturbing the gas flow.

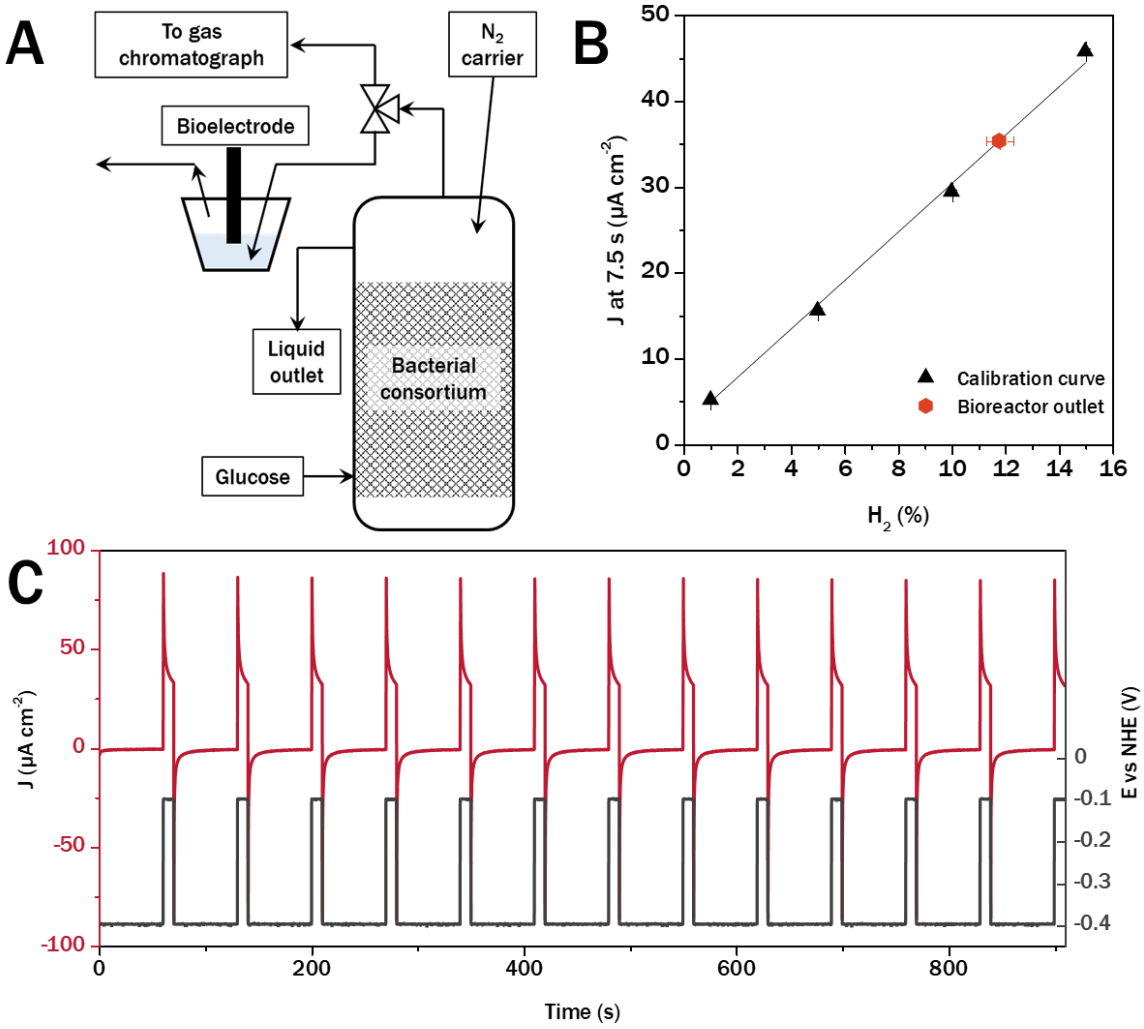

Figure 8. Hydrogen detection in the bioreactor. (A) Scheme of the connection of the electrochemical cell to the bioreactor; (B) Calibration curve for the pulsed hydrogen detection at 7.5 s with the value detected in the bioreactor outlet superimposed; (C) Evolution of the current and potential during the hydrogen detection in the bioreactor gas outlet at the stationary conditions.

The measurements were started 7 days after the inoculation step, when the bioreactor was in steady-state. The gas chromatography measurements right before the biosensor connection and immediately after demonstrated similar gas composition (Table S2) proving that the electrochemical cell connection did not alter the bioreactor behaviour. Nitrogen carrier gas was constantly flushed through the reactor to ensure H_2 gas stripping but also resulting in an approximately 4 times dilution of the biogas. This allowed notably to reach the H_2 concentrations falling within the biosensor linear range.

After the initial solution saturation during 15 min, the CV was recorded. The CV of the bioelectrode in the biogas-saturated buffer solution demonstrated a shape of the catalytic current

similar to those obtained in the cell saturated with 100 % H_2 but with lower magnitude consistent with lower H_2-content in the biogas (Figure S12). The only difference was the appearance of a reduction peak at -0.22 V on the backward scan. This peak persisted during all the experiments but did not change its magnitude nor interfere with *Aa* Hase catalytic current. Further experiments are required to identify the biogas component leading to this peak appearance.

To quantify the H_2-content in the bioreactor gas, the detection was performed in the pulsed mode without any convection. 13 10s-pulses were performed with 60s-intervals between the pulses to permit the diffusion layer renewal (Figure 8C). Since the expected hydrogen concentration exceeded 10 %, the current was sampled at 7.5 s after the pulse beginning to extend the linear range. The pulse current remained stable over more than 15 min of the detection experiment, and the standard deviation of the current calculated over all 13 pulses was 0.7%. Using this current value and the calibration curve (Figure 8B) the hydrogen concentration found in the biogas was estimated to be 11.8 ± 0.5 %. This value correlates well with 12.1 ± 0.1 %, an average of four points measured before and after the bioelectrode connection (Table S2) found using the gas chromatography just before the beginning of the bioelectrode measurement. This proves the feasibility of the developed bioelectrode use for the hydrogen detection in the bioreactor outlet.

Conclusions

We reported the fabrication of an amperometric enzymatic bioelectrode based on a thin CNT-layer on which [NiFe]-hydrogenase from *A. aeolicus* is immobilised. The fabrication process was kept simple and consisted in the drop-coating of the electrode by MWCNT-NH_2 and adsorption of the enzyme from the enriched protein sample. Both the adsorption time and the amount of the deposited enzyme were optimised. The amount of *Aa* Hase as low as 35 pmol/cm^2 was enough to achieve the optimal current densities in these conditions. The unique properties of this hydrogenase, such as thermophilicity and oxygen-tolerance, not only permit to omit the glovebox usage but also make it possible to construct a robust bioelectrode and envision real applications. The thermophilic *Aa* Hase is one the most stable enzymes in its class that allows to envision use of the biosensor even at elevated temperatures.

An original pulsed method developed here can ensure the detection of low amounts of H_2 with high sensitivity and without additional energy input required to enhance the hydrogen mass-transfer. The detection of even smaller hydrogen traces below 1% is also possible with the *Aa*

Hase, which has a low K_M of 1.3 %, but it will require an artificial convection to enhance the flux of H_2 towards the electrode to produce a significant current density. To solve this issue and to improve the general biosensor design, the developed bioelectrode can be replaced by a gas-diffusion bioelectrode featuring the same enzymatic catalyst. This should permit to achieve a higher sensitivity thanks to the proximity of the gas-phase to the catalyst. In addition, the gas-diffusion based design will eliminate the need to saturate the electrolyte solution with the analyte gases thus improving the response time of the biosensor.

Even in the current state, the limit of detection of the developed bioelectrode was below the lower explosion limit of the hydrogen that allows to consider it for the leak detection applications. Nevertheless, in this work we decided to target the hydrogen quantification at the outlet of an anaerobic fermentation bioreactor allowing to imagine a fully sustainable system. We demonstrated that the main co-products of the anaerobic fermentation, CO_2 and H_2S do not interfere with the hydrogen quantification within the range of concentrations expected in the bioreactor gas mixture. Thanks to this and for the first time, we were able to employ the developed biosensor for the quantification of the hydrogen produced in a sustainable way directly at the outlet of the bioreactor. The results of the detection correlated well with the data obtained by an independent method of gas chromatography which proves that the developed biosensor can be successfully used for such complex tasks.

Acknowledgements

This work was supported by National Research Agency (ANR, France) under the grants ANR-19-CE05-0017 and ANR-22-CE50-0004. This work also received support from the French government under the France 2030 investment plan, as part of the *Initiative d'Excellence d'Aix-Marseille Université – A*MIDEX* (AMX-21-PEP-001). T.K. and V.S. are grateful to the Institute of Microbiology, Bioenergies and Biotechnology (IM2B, AMX-19-IET-006) for the internship scholarships.

The authors are grateful to the fermentation (M. Bauzan), protein production (D. Byrne) and microscopy platforms (A. Kosta and H. Le Guenno) of the IMM institute (Marseille, France). The authors thank V. Fourmond for the discussion on the CO_2 equilibrium and P. Infossi for the help with the enzyme purification.

Accepted Manuscript arising from this submission, in accordance with the grant's open access conditions.

Bibliography

Akhlaghi, N., Najafpour-Darzi, G., 2020. Int. J. Hydrogen Energy 45, 22492–22512.

Alonso-Lomillo, M.A., Rüdiger, O., Maroto-Valiente, A., Velez, M., Rodríguez-Ramos, I., Muñoz, F.J., Fernández, V.M., De Lacey, A.L., 2007. Nano Lett. 7, 1603–1608.

Barca, C., Ranava, D., Bauzan, M., Ferrasse, J.-H., Giudici-Orticoni, M.-T., Soric, A., 2016. Bioresour. Technol. 221, 526–533.

Barca, C., Soric, A., Ranava, D., Giudici-Orticoni, M.-T., Ferrasse, J.-H., 2015. Bioresour. Technol. 185, 386–398.

Benomar, S., Ranava, D., Cárdenas, M.L., Trably, E., Rafrafi, Y., Ducret, A., Hamelin, J., Lojou, E., Steyer, J.-P., Giudici-Orticoni, M.-T., 2015. Nat. Commun. 6, 6283.

Brar, K.K., Cortez, A.A., Pellegrini, V.O.A., Amulya, K., Polikarpov, I., Magdouli, S., Kumar, M., Yang, Y.-H., Bhatia, S.K., Brar, S.K., 2022. Int. J. Hydrogen Energy 47, 37264–37281.

Brugna-Guiral, M., Tron, P., Nitschke, W., Stetter, K.-O., Burlat, B., Guigliarelli, B., Bruschi, M., Giudici-Orticoni, M.T., 2003. Extremophiles 7, 145–157.

Ciaccafava, A., De Poulpiquet, A., Infossi, P., Robert, S., Gadiou, R., Giudici-Orticoni, M.T., Lecomte, S., Lojou, E., 2012a. Electrochim. Acta 82, 115–125.

Ciaccafava, A., De Poulpiquet, A., Techer, V., Giudici-Orticoni, M.T., Tingry, S., Innocent, C., Lojou, E., 2012b. Electrochem. commun. 23, 25–28.

Darmadi, I., Nugroho, F.A.A., Langhammer, C., 2020. ACS Sens 5, 3306–3327.

Felbek, C., Arrigoni, F., de Sancho, D., Jacq-Bailly, A., Best, R.B., Fourmond, V., Bertini, L., Léger, C., 2021. ACS Catal. 11, 15162–15176.

Ghimire, A., Frunzo, L., Pirozzi, F., Trably, E., Escudie, R., Lens, P.N.L., Esposito, G., 2015. Appl. Energy 144, 73–95.

Hidalgo, D., Martín-Marroquín, J.M., 2022. JOM (1989).

Hitaishi, V.P., Clément, R., Quattrocchi, L., Parent, P., Duché, D., Zuily, L., Ilbert, M., Lojou, E., Mazurenko, I., 2020. J. Am. Chem. Soc. 142, 1394–1405.

Hübert, T., Boon-Brett, L., Black, G., Banach, U., 2011. Sens. Actuators B Chem. 157, 329–352.

Léger, C., Dementin, S., Bertrand, P., Rousset, M., Guigliarelli, B., 2004. J. Am. Chem. Soc. 126, 12162–12172.

Li, Q., Lancaster, J.R., Jr, 2013. Nitric Oxide 35, 21–34.

Lojou, É., Giudici-Orticoni, M.-T., Bianco, P., 2005. J. Electroanal. Chem. (Lausanne Switz) 577, 79–86.

Lubitz, W., Ogata, H., Rüdiger, O., Reijerse, E., 2014. Chem. Rev. 114, 4081–4148.

Luo, X., Brugna, M., Tron-Infossi, P., Giudici-Orticoni, M.T., Lojou, E., 2009. J. Biol. Inorg. Chem. 14, 1275–1288.

Lutz, B.J., Fan, Z.H., Burgdorf, T., Friedrich, B., 2005. Anal. Chem. 77, 4969–4975.

Mazurenko, I., Monsalve, K., Infossi, P., Giudici-Orticoni, M.-T., Topin, F., Mano, N., Lojou, E., 2017. Energy Environ. Sci. 10, 1966–1982.

Mazurenko, I., Monsalve, K., Rouhana, J., Parent, P., Laffon, C., Goff, A.L., Szunerits, S., Boukherroub, R., Giudici-Orticoni, M.-T., Mano, N., Lojou, E., 2016. ACS Appl. Mater. Interfaces 8, 23074–23085.

McArdle, T., McNamara, T.P., Fei, F., Singh, K., Blanford, C.F., 2015. ACS Appl. Mater. Interfaces 7, 25270–25280.

Monsalve, K., Mazurenko, I., Gutierrez-Sanchez, C., Ilbert, M., Infossi, P., Frielingsdorf, S., Giudici-Orticoni, M.T., Lenz, O., Lojou, E., 2016. ChemElectroChem 3, 2179–2188.

Multi-Year Research, Development, and Demonstration Plan 2011−2020. Section 3.7 Hydrogen Safety, Codes and Standards, 2015. . U.S. Department of Energy (DOE).

Nel ASA: Status update #5 regarding incident at Kjørbo [WWW Document], 2019. . Nel Hydrogen. URL https://nelhydrogen.com/press-release/nel-asa-status-update-5-regarding-incident-at-kjorbo/ (accessed 10.4.22).

Oteri, F., Ciaccafava, A., de Poulpiquet, A., Baaden, M., Lojou, E., Sacquin-Mora, S., 2014. Phys. Chem. Chem. Phys. 16, 11318–11322.

Pandelia, M.-E., Infossi, P., Giudici-Orticoni, M.T., Lubitz, W., 2010. Biochemistry 49, 8873–8881.

de Poulpiquet, A., Ciaccafava, A., Gadiou, R., Gounel, S., Giudici-Orticoni, M.T., Mano, N., Lojou, E., 2014. Electrochem. commun. 42, 72–74.

Qian, D.-J., Nakamura, C., Wenk, S.-O., Ishikawa, H., Zorin, N., Miyake, J., 2002. Biosens. Bioelectron. 17, 789–796.

RenNanqi, GuoWanqian, LiuBingfeng, CaoGuangli, DingJie, 2011. Curr. Opin. Biotechnol. 22, 365–370.

Rodríguez-Maciá, P., Reijerse, E.J., van Gastel, M., DeBeer, S., Lubitz, W., Rüdiger, O., Birrell, J.A., 2018. J. Am. Chem. Soc. 140, 9346–9350.

Sarangi, P.K., Nanda, S., 2020. Chem. Eng. Technol. 43, 601–612.

Staffell, I., Scamman, D., Velazquez Abad, A., Balcombe, P., Dodds, P.E., Ekins, P., Shah, N., Ward, K.R., 2019. Energy Environ. Sci. 12, 463–491.

Tee, S.Y., Win, K.Y., Teo, W.S., Koh, L.-D., Liu, S., Teng, C.P., Han, M.-Y., 2017. Adv. Sci. (Weinh.) 4, 1600337.

Vincent, K.A., Belsey, N.A., Lubitz, W., Armstrong, F.A., 2006. J. Am. Chem. Soc. 128, 7448–7449.

Vincent, K.A., Parkin, A., Armstrong, F.A., 2007. Chem. Rev. 107, 4366–4413.

Xu, X., Zhou, Q., Yu, D., 2022. Int. J. Hydrogen Energy 47, 33677–33698.